AUTOMATED EXTRACTION OF FLOOD FOR LARGE SCALE AREA USING WEIGHT AVERAGE OTSU'S METHOD FROM ALOS-2 DUAL POLARIZATION AND MODIS

Husniyah Binti Mahmud (1), Masahiko Nagai (1)
[1] Yamaguchi University, 16-1 Tokiwadai 2-chome, Ube-shi, 755-8611 Yamaguchi
Email: i504wd@yamaguchi-u.ac.jp; nagaim@yamaguchi-u.ac.jp

KEY WORDS: Flood, ALOS-2, Polarisation, Automatic detection, OTSU

ABSTRACT: The massive impact of the flood has been a great concern of Malaysia for many years. The applications of satellite precipitation products have been widely accepted as a monitoring tool. This study evaluated the potential of satellite ALOS-2 dual polarization to automatically monitor flood condition in northwest Malaysia. An automated flood extraction system by using weight averages of local Otsu's threshold values using total backscatter of HH and HV of ALOS-2 images was carried out. ALOS-2 with MODIS satellite images derived indices validated to measure the consistency and discrepancies between both satellites. Spatio-temporal water movement during start date and end date of 2017 flood using ALOS-2 and MODIS were monitored. The results indicated; (1) total backscatter of HH and HV gives a good automatic water surface extraction due to higher frequency of bimodal histogram with range 73.53 % to 85.53% compared to HH backscattering (55.88 % to 83.82 %), (2) Flood spatial extent of ALOS-2 and MODIS shows good agreement with r = 0.88. However, due to the different sensor and spatial resolution, ALOS-2 gives more detailed and precise result, (3) The extraction result of 2017 flood, using HH+HV water move from the center to the northern and flooding occur over a long duration because of the low land area. Therefore, the flood extent and duration map is very important for flood control and remedial.

1. INTRODUCTION

In Malaysia flood is the most severe natural disaster. Based on Annual flood report for the year 2016/2017 by DID, estimated 404 flood events have been reported throughout Malaysia region with USD12,649,379.84 economic loss and 95,929 evacuated from their home (DID, 2018). There are two types of flood commonly take place in Malaysia, which are monsoon flood and flash flood. Intense rainfall commonly caused by Northeast monsoon that occurs from November to March impacted east coast of Peninsular Malaysia, the northern part of Sabah and southern part of Sarawak.

Phased Array type L-band Synthetic Aperture Radar (PALSAR) onboard Advanced Land Observing Synthetic (ALOS) retrieve information by emitting microwave and receive the reflection from the ground. PALSAR able to provide less affected cloud satellite image during day and night in any weather condition. The first PALSAR was launch on 24th January 2006 and complete its operation on 12th May 2011. The mission continued by ALOS-2 PALSAR-2 from 24th May 2014. PALSAR-2 was utilized to detect flood in this study due to its ability to provide observe the land in any weather condition. Beside, radar data can recognize smooth open water areas because flat-water surface behaves as specular reflectors and scatter the radar pulse back to the antenna. Water area will appear dark which can further be differentiated from non-water area.

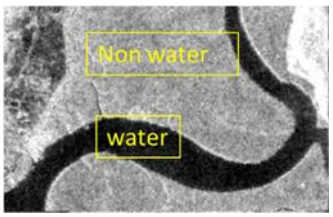

Figure 1 Coarse surface have high backscattering value and appear bright while smooth surface will have low backscattering and appear dark.

Multipolarized L-band can transmit and receive radar in a linear like polarized: horizontal transmit,

horizontal receive (HH); vertical transmit, vertical receive (VV); and cross-polarized; horizontal transmit, vertical receive (HV); and vertical transmit, horizontal receive (VH). The polarized radar system can impact the strength of the backscatter and can detect submerge cropped area compare to single polarized radar data. Potential of HH and HV dual-polarization evaluated in this study.

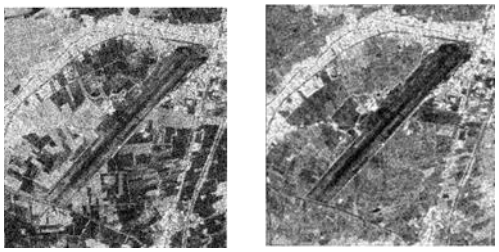

Figure 2 HH polarization (left) HV polarization (right)

For determination of water and flood areas single co polarization HH (horizontal transmit and horizontal receive) SAR images have been used in many previous studies because it enhances the contrast between forest and flooded vegetation and maximizes canopy penetration [2, 3]. However, during the presence of wind HV (horizontal transmit vertical receive) can give a better result of water extraction since, cross-polarized less affected by wind than co-polarized HH [2, 3]. Therefore, dual-polarization has the potential to improve the effectiveness of water extraction.

The objectives of this study are to establish an automated surface water extraction system by using averages of local Otsu's threshold values using total backscatter of HH and HV of ALOS-2. MODIS 09A1 derived indices used for validation and to monitor spatial-temporal water movement during start date and end date of 2017 flood.

2. MATERIALS AND METHOD

2.1 Description of study area

Study area in this study lies around the northwest of peninsular Malaysia which included Perlis and Kedah states. As shown in Fig. 4, the study area covers about 5.35N to 6.35N longitude and 99°46'3.22"E to 99°59'25.07"E latitude. Northwest Malaysia is the largest paddy planting area in Malaysia. In general, the climatic regime in Northwest Malaysia is a regular dry season that stays around 2 to 4 months from December to March. The first period of the rainy season is from September to November and the second period is from April to May.

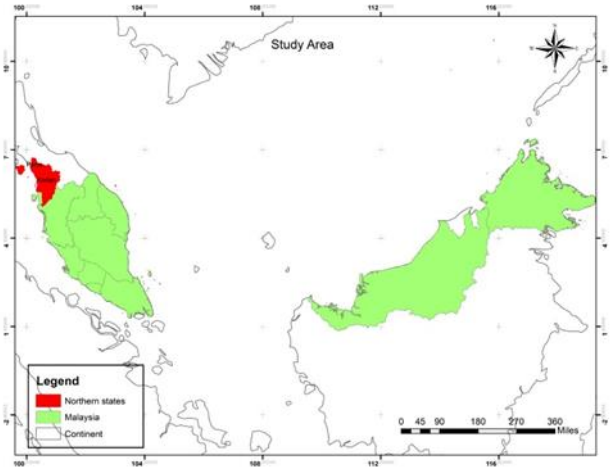

Figure 4 Study area

2.2 Satellite data

In this study, PALSAR-2 and MODIS data are utilized. Table 1 summarizes the description of PALSAR-2. In total, there are 18 PALSAR-2 images with ascending mode, with a constant off-nadir angle of 32.9°, a spatial resolution of 6.25m and in dual-polarization HH and HV are selected. PALSAR-2 data was ordered from https://auig2.jaxa.jp.

Table 1. Utilized PALSAR-2 data.

Satellite/ sensor	Pass	Frame	Polarization mode	Observation Date
ALOS-2 PALSAR-2	Ascending	100 -110	HH/HV	October 2, 2014 February 19, 2015 October 1, 2015 February 18, 2016 September 29, 2016 February 16, 2017 September 28, 2017 February 1, 2018 March 1, 2018

MODIS MOD09A1 500m resolution with an 8-day composite from Terra (MOD09A1) datasets covering study area is used in this study. MODIS MOD09A1 was downloaded from https://search.earthdata.nasa.gov.

2.3 Data analysis

Figure 5 shows the flowchart of Spatial-temporal water movement detection. Initially, PALSAR-2 image preprocessed using Sentinel Application Platform (SNAP) software. Preprocessed of PALSAR-2 image involve merge of two PALSAR-2 frames to cover study area, calculation of beta Nought, Lee speckle filtering with 5x5 windows and sigma Nought calculation. Afterward, each co polarized HH (horizontal transmit and horizontal receive) image and dual-polarized which is total backscatter of HH and HV cut into small specific water references. The criteria of water references explained in the next section. Histogram, OTSU, and modification of OTSU image thresholding (Valley Emphasis (VE) and Neighborhood Valley Emphasis (NE)) of each water references determined fully automatic by developing Python script with software libraries like GDAL and Numpy.

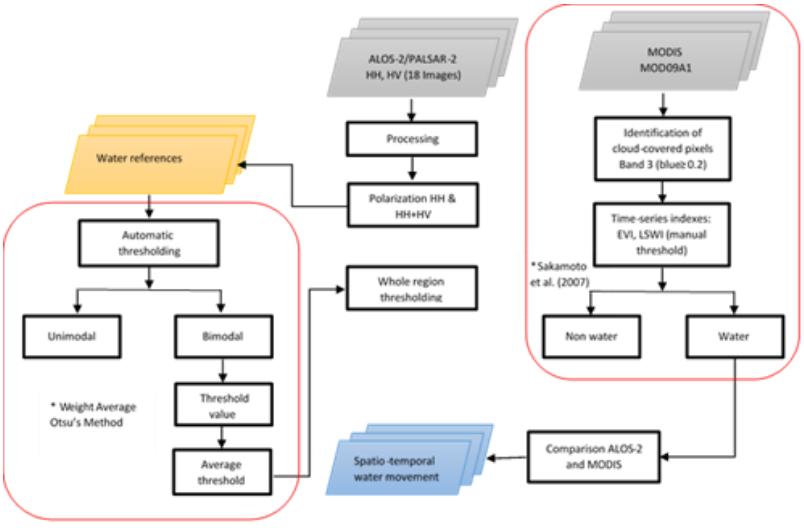

Figure 5 Flowchart of spatial-temporal water movement detection

OTSU, VE and NE threshold value of each water references with bimodal shape used for averaging

to represent the whole region threshold while unimodal histogram rejected for next processed. Among the water extraction map from each average OTSU, VE and NE image threshold was compared and the most precise segmented image was selected for the final representation of water movement map.

Optical satellite image MODIS MOD09A1 used for comparing with PALSAR-2 and temporal gap filling for detection of water movement during the flood event. Determination of threshold of water and non-water for MODIS was done using QGIS software with semi-automatic way. Decision tree from Sakamoto et al. (2007) was adopted and modified to categorize each MODIS pixel into water and non-water related pixels.

First, pixels of blue reflectance or band 3 with value ≥ 0.2 identified as cloud-related pixels and removed from the image. Next, EVI, LSWI, and the difference between the value of EVI and LSWI were calculated. If pixels of EVI and LSWI difference less than or equal to 0.05 and EVI≤ 0.3 with EVI≤0.05 and LSWI≤0.05, the pixels considered as water-related pixels.

2.4 Selection of water references

All the water references were selected using the following criteria proposed by Pisut et al. (2017): having an area larger than 320000m2 (8192 pixels for a resolution 6.25m), containing water throughout the year, not facing a flood situation, located on flat ground as much as possible, and having water and non-water cover ratio of nearly 1:1. An irregular shape was allowed. In this study, a circle shape is used to maintain the ratio of water and non-water 1:1 ratio.

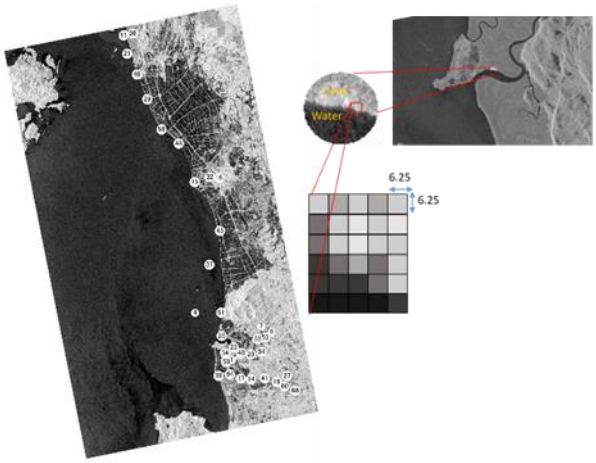

Figure 6 Distribution of water references throughout study area and criteria used for selection

The 68 water references were selected from different types of water bodies, natural and man-made. The locations water references distribution and criteria are shown in Fig. 6.

2.5 Weight average Otsu's Method

Image thresholding involves converting grayscale image (f(x,y)) to binary image (g(x,y)) where pixels value lower than threshold classified as zero while pixels higher than threshold classified as one. In general, this can be simplified as follows:

$$(x, y) = \begin{cases} 1 & \text{if } f(x,y) \geq T \\ 0 & \text{otherwise,} \end{cases} \qquad (3)$$

(1) First, to compute the OTSU threshold, the histogram of the pixels computed. Probability of threshold, T determined by dividing gray image pixels into the background, b and foreground, p. Then, the weight of background, wb and foreground pixels, wp calculated by dividing the total of background pixels frequency, fb with the total number of entire pixels as follows:

$$\mathrm{W}_b\ (Weight\ background) = \frac{f_{b1}+f_{b2}+\cdots f_n}{Total\ number\ of\ entire\ pixels}\ , (4)$$

$$W_\mathrm{p}\ (Weight\ foreground) = \frac{f_{p1}+f_{p2}+\cdots f_n}{Total\ number\ of\ entire\ pixels}\ , (5)$$

(2) Secondly, the mean of background and foreground pixels calculated by adding multiplication of background pixels frequency, fb with its pixels value Vb and divide with the sum of background pixels. The calculation is as follows:

$$\mu_\mathrm{b}\ (Mean\ background) = \frac{(f_{b1}*v_{b1})+(f_{b2}*v_{b2})+\cdots(f_n*v_n)+(f_n*v_n)}{Total\ number\ of\ background\ pixels}, (6)$$

$$\mu_\mathrm{p}\ (Mean\ foreground) = \frac{(f_{p1}*v_{p1})+(f_{p2}*v_{p2})+\cdots(f_n*v_n)+(f_n*v_n)}{Total\ number\ of\ foreground\ pixels}\ , (7)$$

(3) The variance of background pixels and foreground pixels calculated by averaging square distance background frequency pixels with the mean background

$$V_b(Variance\ background) = \frac{((f_{b1}-\mu_b)^2*v_{b1})+((f_{b2}-\mu_b)^2*v_{b2})\ldots.((f_n-\mu)^2*v_n)+((f_n-\mu)^2*v_n)}{\text{Total number of background pixels}}, \quad (8)$$

$$V_p(Variance\ foreground) = \frac{\left((f_{p1}-\mu_p)^2*v_{p1}\right)+\left((f_{p2}-\mu_p)^2*v_{p2}\right)\ldots.((f_n-\mu)^2*v_n)+((f_n-\mu)^2*v_n)}{Total\ number\ of\ \text{foreground}\ pixels}, \quad (9)$$

(4) Afterward, the within-class variance was calculated by totaling background and foreground variance multiplied with their weights.

$$\text{Within class variance} = W_bV_b + \mathrm{W}_fV_f\ , \quad (10)$$

Where

$$\mu = W_b\mu_b + W_f\mu_f, \quad (11)$$

(6) Valley Emphasis (VE) thresholding calculated by multiplying maximal between class variance with inverse proportional to the probability of at threshold, T.

$$\mathrm{VE} = \text{Maximal between class variance} * (1 - \mathrm{p_T}), \quad (12)$$

(7) Neighborhood Emphasis (NE) thresholding calculated by

$$\mathrm{NE} = \text{Maximal between class variance} * \sum_{\mathrm{i}=-\mathrm{m}}^{\mathrm{m}}(1 - \mathrm{p_T}), \quad (13)$$

3. RESULTS AND DISCUSSION

3.1 Automated thresholding with OTSU, VE and NE technique

By considering the peaks, valleys, and curvatures of the smoothed histograms, the water references with unimodal distributions were rejected, and only those with bimodal distributions were taken into account. The weight average value of the automated threshold for each OTSU, VE and NE technique display on each whole HH PALSAR-2 image histogram in Fig.7.

Figure 7 The weigh average of HH applied on the whole area Green indicate OTSU threshold, Purple shows VE threshold and Red represent NE threshold

Fig. 8 shows the histogram of HH+HV PALSAR-2 with applied weight average of OTSU, VE and NE.

Figure 8 The weigh average of HH+HV applied on the whole area Green indicate OTSU threshold, Purple shows VE threshold and Red represent NE threshold

Based on Fig. 7 by applying OTSU on the HH image the threshold value is not accurately located at the valley of the histogram compare with Fig. 8 whereby using HH+HV threshold value mostly located at closest valley point of the histogram.

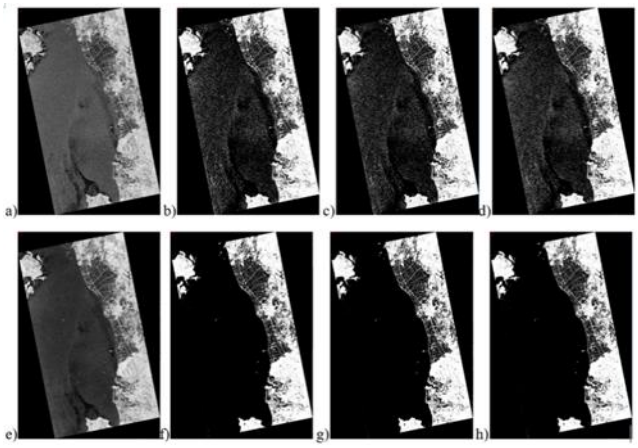

Figure 9 Extracted result of weight average from the image acquired on 02 October 2014 (a) preprocessed HH (b) OTSU HH (c) VE HH (d) NE HH (e) preprocessed HH+HV (f) OTSU HH+HV (g) VE HH+HV (h) NE HH+HV

The image segmentation by using OTSU, VE and NE were used to simply extract water surface by applying a global threshold value to each PALSAR-2 image. Fig. 9 shows 2nd October 2014 as the sample image of the extracted result. OTSU threshold of HH image = 48.4 while, OTSU threshold of HH+HV = 84.3. The result shows that HH+HV gives better surface water extraction compared to HH. By using the VE technique, the threshold of HH = 48.5 and threshold of HH+HV= 84.6. While,

NE weight average threshold for HH image = 48.0 and HH+HV image = 83.4. The range of each threshold technique for every single image indistinct with each other.

Based on Fig. 9, HH+HV image separated the object clearly with more object details than HH image. OTSU, VE, and NE technique do not give a significant impact on separating the object with the background. In this study, the threshold from NE technique as recommended by Jiu-Lun Fan et. al, 2012 selected to compared with MODIS and represent water movement during the flood event.

Table 2. Automatic threshold values using the NE technique of water reference with circle areas from the HH and HH + HV sigma-naught values taken on the evening of 02 October 2014 5.30 PM until 01 March 2018 5.30 PM.

Local Time	Pass	Beam	Number of Water References	Bimodal Threshold HH		Bimodal Threshold HH+HV	
			Count	Bimodal (%)	Weigh Average	Bimodal (%)	Weigh Average
2014/10/02 17:30	Ascending	FBD	68	67.64	47.97	80.88	83.44
2015/02/19 17:30	Ascending	FBD	68	66.18	49.05	73.53	84.50
2015/10/01 17:30	Ascending	FBD	68	72.06	50.86	77.94	85.93
2016/02/18 17:30	Ascending	FBD	68	57.35	48.65	80.88	84.11
2016/09/29 17:30	Ascending	FBD	68	67.65	51.18	80.88	87.89
2017/02/16 17:30	Ascending	FBD	68	55.88	51.26	83.82	87.66
2017/09/28 17:30	Ascending	FBD	68	69.12	134.93	80.88	145.53
2018/02/01 17:30	Ascending	FBD	68	83.82	42.90	85.29	78.09
2018/03/01 17:30	Ascending	FBD	68	67.65	52.27	79.41	86.02

As seen in Table 2, the bimodal percentage number indicates the occurrence probability of the bimodal distribution for each image. Thus, HH + HV is more likely to have a bimodal distribution with 73%-85% and is more suitable for automatic classification compares to HH that has percentage 56%-72% to get bimodal distribution. In other words, the HV polarization can improve the efficiency of water surface extraction. Thus, the extracted water areas presented in this study were derived from HH + HV.

Some of the close-ups of the extracted result from the HH+HV image acquired on 2nd October 2014 with NE threshold value are shown in Figure 10. The water boundaries obtained using this technique appear to be reasonable. The results of the water area are shown in white, and the non-water area shown in blue. There are some errors in waterline area positions due to side-looking geometry of the SAR sensors cause shadowing, foreshortening and layover effects and underestimation of the waterline.

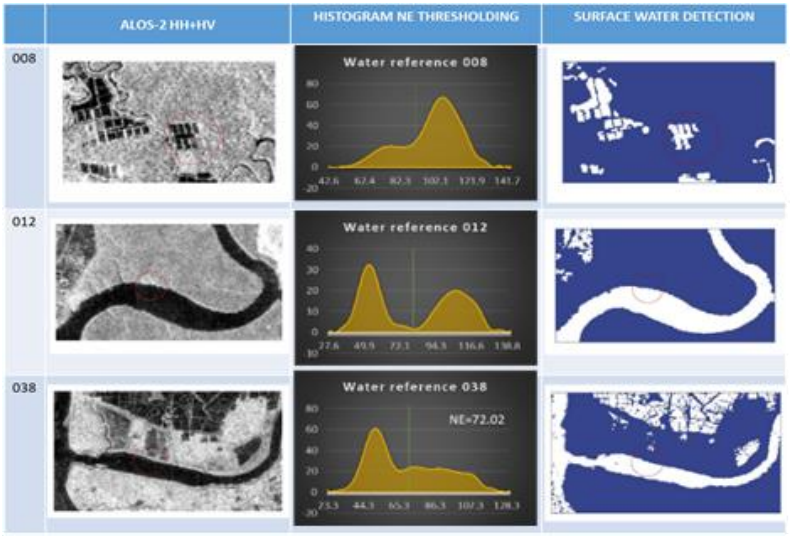

Figure 10 Automated threshold values using the neighborhood valley method of water references in the red elliptical areas (3 of 68) from the HH and HH + HV sigma-naught values taken on the evening of 02 October 2014 5:30 PM. The solid green line represents NE threshold value.

3.2 Automated thresholding with OTSU, VE and NE technique

Figure 11 shows a comparison of ALOS-2 and MODIS satellite data give a high correlation with value 0.88.

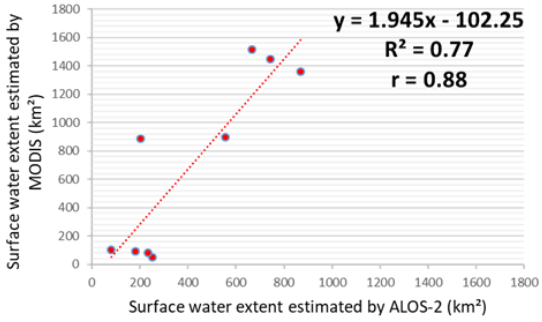

Figure 11 Correlation of Area of surface water detected by PALSAR-2 and MODIS

Figure 11 shows during dry period ALOS-2 overestimated area of surface water compare to MODIS. In contrast, during wet seasons, ALOS-2 underestimate the surface water area compares to MODIS. In between 2014 to 2018, the highest surface water extracted by MODIS is on September 2017 with 1517.57km². While for ALOS-2 the highest extracted water surface was on 2014 with 868.92km². A comparison of ALOS-2 and MODIS satellite data shows a high correlation with value 0.88.

3.3 Water movement for 2017 flood

The flood duration map was produced by stacking the interval of the extracted water surfaces. The final flood duration map is shown in Figure 13 and pink color indicate current flood while purple color shows previous flood extent.

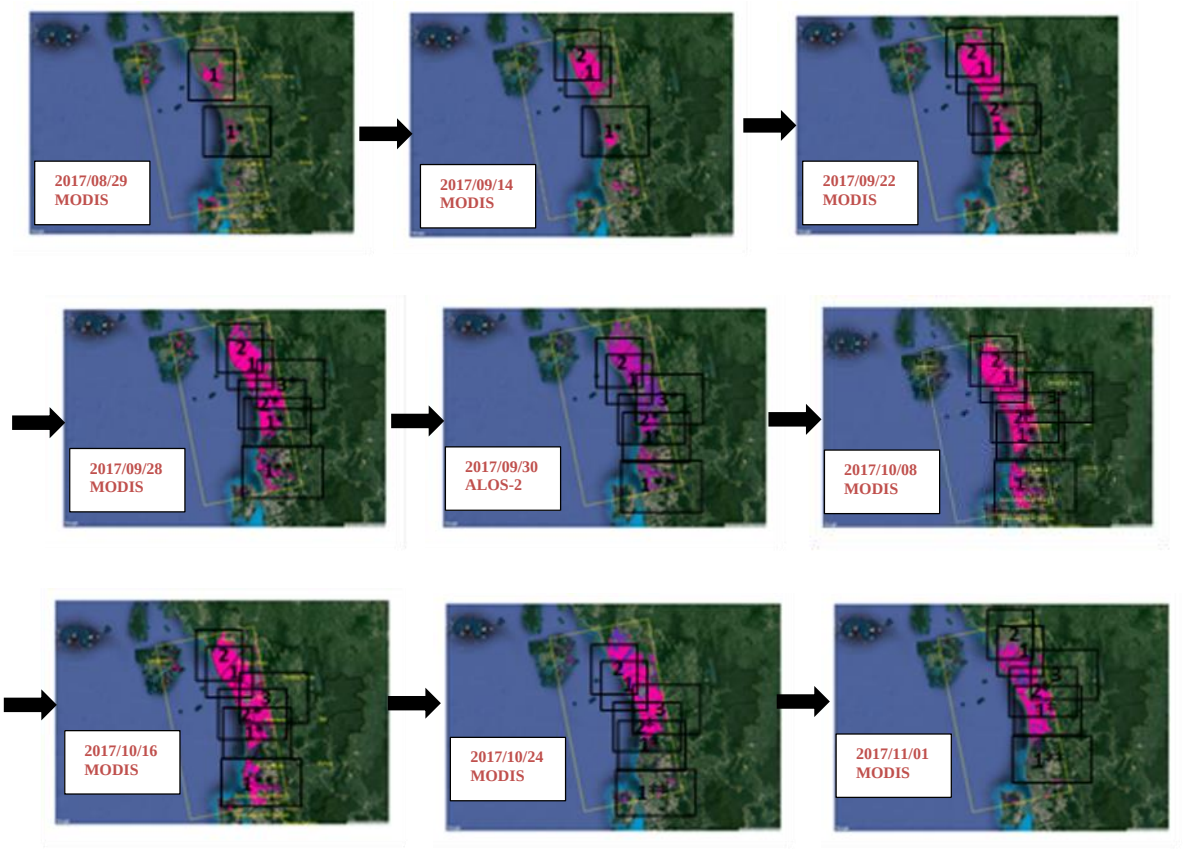

Figure 12 the 2017 flood duration map

Figure 12 shows 2017 flood duration map at the study area and on 2017/08/29, water accumulated at point 1 and 1*. From point 1, the water moves to the northern region approximately at point 2 on 2017/09/14 and on 2017/09/22 onward, the flood at point 1* gradually grow. On 2017/09/28, from point 2, the water moves slightly to the northern area. Eventually, these two flood region area combined, while, for the bottom part, it moves to the eastern region 3. New flooded region emerges at point 1**. On 2017/09/30, ALOS-2 image was used and the fusion of PALSAR-2 and MODIS shows consistent flood border but due to the different sensor and spatial resolution. The spatial extent remains the same from 2017/10/08 to 2017/10/16. Surface water at some top region slightly recedes while at point 1** surface water diminishes. On 2017/11/01, the water gradually drain away at the remaining region.

4. CONCLUSION

HH+HV grayscale image has a higher frequency of bimodal distribution with range 73.53 % to 85.53% compare to HH backscattering with 55.88 % to 83.82 % frequency bimodal. Thus, HH+HV chosen for automatic thresholding using NE OTSU. This technique provides a satisfactory water extraction result. Flood spatial extent of ALOS-2 and MODIS shows good agreement with r = 0.88. However, due to different sensor and spatial resolution, ALOS-2 gives a more detailed and precise result. The extraction result of 2017 flood, using HH+HV water move from the center to the northern and flooding occur over a long duration because of the low land area. Therefore, the flood duration map is very important for flood control and remedial.

Acknowledgments

We would like to express our gratitude to the Japan Aerospace Exploration Agency (JAXA) for providing ALOS-2 data. We would also like to thank people that assist and give comments that greatly improved the research.

References from Journals:

Department of Drainage and Irrigation. Laporan Tahunan Bagi Tahun 2016/2017. 2018.

Behnamian, A., Banks, S., White, L., Brisco, B., Milard, K., Pasher, J., … Battaglia, M., 2017. Semi-automated surfacewater detection with synthetic aperture radar data: A wetland case study. Remote Sensing, 9(12), 1–21. http://doi.org/10.3390/rs9121209.

Bolanos, S., Stiff, D., Brisco, B., & Pietroniro, A., 2016. Operational surface water detection and monitoring using Radarsat 2. Remote Sensing, 8(4). http://doi.org/10.3390/rs8040285.

Nakmuenwai, P.; Yamazaki, F.; Liu, W. Automated Extraction of Inundated Areas from Multi-Temporal Dual Polarization RADARSAT-2 Images of the 2011 Central Thailand Flood. Remote Sens. 2017, 9, pp 78.

Sakamoto, T.; N.V. Nguyen,; A. Kotera,; H. Ohno,; N. Ishitsuka,; and M. Yokozawa. Detecting temporal changes in the extent of annual flooding within the Cambodia and the Vietnamese Mekong Delta from MODIS time-series imagery, Remote Sensing of Environment, 2007, pp 295–313.

Fan, J.; Lei, B. A modified valley-emphasis method for automatic thresholding. Pattern Recogn. Lett. 2012, 33, pp 703–708.